Effect of DVI Nozzle Location on the Thermal Mixing in the RVDC

Hyung Seok Kang*1, Bong Hyun Cho, Hwan Yeol Kim, Juhyeon Yoon, Yoon Yeong Bae

DVI 노즐 위치가 원자로 하향유로내의 냉각수 열적혼합에 미치는 영향 분석

강 형 석, 조 봉 현, 김 환 열, 윤 주 현, 배 윤 영

한국형 차세대원자로에서는 비상노심 안전주입수가 저온관을 통하지 않고 원자로용기에 직접 주입된다. 원자로용기의 가압열충격과 열수력적 관점에서 최적의 노즐위치를 결정하기 위해서 전산유체역학을 활용하였다. 상용 전산유체코드인 CFX를 이용하여 원자로 하향유로를 모사하는 해석대상 격자를 다중불록으로 형성한 다음 유동장을 비압축성 Navier-Stokes 운동량 방정식, 에너지 방정식과 표준 k-ε 난류모형 등으로 모형화하여 3 차원 비정상상태 계산을 수행하였다. CFX 에서는 경계밀착좌표계, 비엇물림격자와 SIMPLE 알고리즘을 사용한다. 본 연구결과 원자로용기의 가압열충격 관점에서 가장 보수적인 사고인 증기관 파단사고시에도 열적혼합이 잘 일어나 가압열충격이 발생할 가능성이 없는 것으로 판단되며 안전주입수 노즐이 저온관 바로 위에 위치할 때 원자로 하향유로 내의 온도 분포가 가장 균일하여 열적 혼합 관점에서는 최적의 위치로 판단된다.

Key Words: 원자로용기 직접주입(Direct Vessel Injection), 전산유체역학(Computational Fluid Dynamics), 다중불록격자(Multi-Block Grid), 비엇물림격자(Non-Staggered Grid), 경계밀착좌표계(Body Fitted Coordinate)

1. Introduction

Direct Vessel Injection(DVI) concept has been introduced as Emergency Core Cooling(ECC) of Advanced Light Water Reactor(ALWR) which satisfies the licensing requirement in USA[1]. However, the flow and temperature pattern during safety injection via DVI nozzle has not been

*1 정회원, 한국원자력연구소

investigated extensively, although there exist some analytical and experimental investigations[2][3][4]. If the fluid temperature around vessel beltline in the Reactor Vessel Downcomer(RVDC) is dropped below RT_{PTS}, 98F, (Reference Temperature-Pressurized Thermal Shock), reactor vessel has the possibility to be exposed to embrittle fracture. Nuclear Steam Supply System (NSSS) design requires that the temperature of vessel beltline should not be decreased abruptly when ECC coolant is injected into the RVDC. The material used for the reactor vessel beltline, shown in Fig. 1, become embrittled due to neutron fluence.

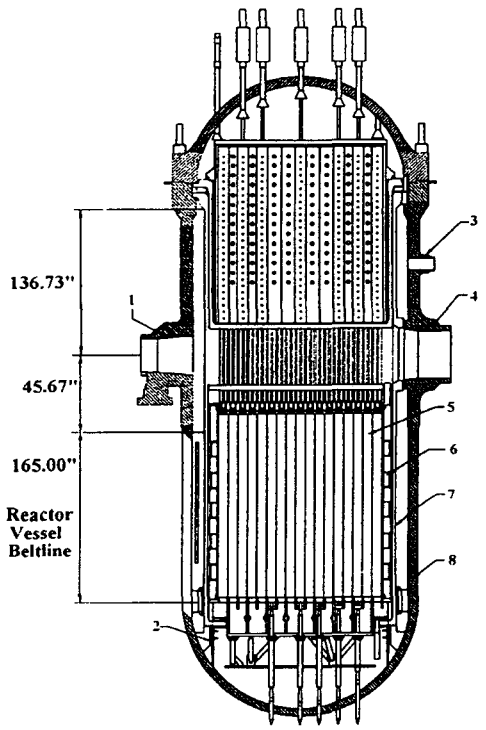

Fig. 1 KNGR Reactor Vessel

1-Cold Leg Nozzle, 2-Flow Skirt, 3-DVI Nozzle, 4-Hot Leg Nozzle, 5-Fuel Assembly, 6-Core Shroud, 7-Core Support Barrel, 8-Reactor Vessel

The temperature distribution in RVDC is determined by the temperature and the flow mixing between injected ECC coolant through DVI nozzle and circulated reactor coolant through cold leg. The temperatures of ECC coolant and reactor coolant depend on the plant characteristics. The degree of mixing will depend on the DVI nozzle location. The main purpose of this study is to recommend the optimum DVI nozzle location which maximizes thermal mixing in RVDC. The computational fluid dynamic code "CFX" is used for this study.

2. Selection of Accidentes to be Analyzed

The events to be evaluated for thermal mixing is carefully chosen from those of lower than the range of Anticipated Operating Occurrence (AOO) in the PWR operation experience. Previous analysis recommends that Main Steam Line Break (MSLB) is the most dangerous accident for PTS[5]. The most conservative accident scenario in the MSLB about PTS is large Reactor Coolant System(RCS) pressure drop, low reactor coolant temperature, maximum ECC injection flow rate and minimum RCS circulation flow. The amount of flow circulation along the affected Steam Generator (SG) loop involving MSLB accident is larger than that of intact SG loop.

The flow circulation of intact SG loop stops at around 540 seconds after MSLB accident occurs. Since ECC injection flow increases RCS pressure drops, zero power operation is more conservative than full power operation. The loss of offsite power with Reactor Coolant Pump (RCP) stop is also a severe condition which induces poor

mixing of ECC injection and reactor coolant circulation flows. Consequently, the most severe conditions for PTS under MSLB are zero power operation, loss of offsite power, no circulation flow in the intact SG loop, and only natural circulation of low temperature coolant through the affected SG loop for 570~600 seconds after MSLB incident.

The results of safety analyses show that the NSSS pressure and temperature is stabilized at around 600 seconds after MSLB incident. Thus, there is no need to analyze the flow field in RVDC after 600 seconds.

3. Analysis

3.1 Geometry Configuration and Grid Generation

Five DVI nozzle locations are carefully selected to determine the optimum location shown in Fig. 2. These five locations are selected based on the literature survey on the results of experiments and numerical analyses and DVI nozzle location of ABB-CE system 80+[2][3][4][5].

The DVI nozzle location of system 80+ is selected as reference case. case 1, and this location is moved toward the cold leg and the hot leg as shown in Fig. 2. The inside diameter of DVI nozzle is assumed to 10.13" because the exact diameter is not determined yet. Based on the above and considering a symmetric flow condition in the RVDC, a half of cylindrical geometry with hot leg, cold leg per each SG loop and two DVI nozzles is constructed. The cold leg and DVI nozzle are assumed to be a regular square for convenience of grid generation. The pre-processor of CFX. CFX-Meshbuild. is used to generate multi-block structured grid. In the grid model, the outlet was extended further downstream (extra calculation domain "D" is added) to apply the fully developed outlet condition as shown in Fig 3., to avoid the difficulties in getting converged solution.

The grid distributions for each DVI nozzle are shown in Table 1 and Fig. 3. The grid nodes region A is more densely distributed than region B, C and D because flow behavior of region A is more complicated. The number of grid nodes is effectively determined considering the computation time and numerical accuracy of trial run.

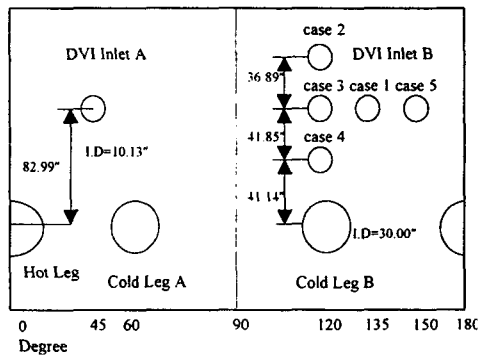

Fi g. 2 Five DVI Nozzle Locations

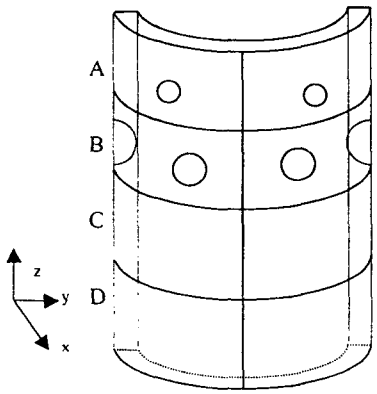

Fig. 3 Schematic Diagram of the Grid Model

Table 1 Distribution of Grid Nodes

		X	Y	Z	Dimension(inch)
Case 1	A	32	6	16	562.10
	B	32	6	8	635.00
	C	32	6	25	1197.10
	D	32	6	20	1197.10
Case 2	A	32	6	16	562.10
	B	32	6	8	635.00
	C	32	6	25	1197.10
	D	32	6	20	1197.10
Case 3	A	32	6	16	562.10
	B	32	6	8	635.00
	C	32	6	25	1197.10
	D	32	6	20	1197.10
Case 4	A	32	6	18	860.72
	B	32	6	8	336.38
	C	32	6	25	1197.10
	D	32	6	20	1197.10
Case 5	A	32	6	16	562.10
	B	32	6	8	635.00
	C	32	6	25	1197.10
	D	32	6	20	1197.10
RVDC thickness					10.13
RVDC inner diameter					162.00

3.2 Numerical Method and Governing Equation

The flow field of RVDC is modeled by incompressible three dimensional Navier-Stokes equation with standard k-ε turbulence model included in CFX[6]. CFX uses body fitted coordinate, non-staggered grid, control volume method and SIMPLE(Semi-Implicit Method for Pressure Linked Equations). Body fitted coordinate systems extend the capabilities of finite difference methods to deal with complex geometry. The basic idea is to use a curvilinear coordinate transformation to map the complex flow domain in physical space to a simple flow domain in computational space as shown in the equations (1), (2).

$$\frac{\partial \phi}{\partial \xi^i} = \frac{\partial x^j}{\partial \xi^i}\frac{\partial \phi}{\partial x^j} = J_i^j \frac{\partial \phi}{\partial x^j} \tag{1}$$

$$\frac{\partial \phi}{\partial x^i} = \frac{\partial \xi^j}{\partial x^i}\frac{\partial \phi}{\partial \xi^j} = \bar{J}_i^j \frac{\partial \phi}{\partial \xi^j} \tag{2}$$

The non-staggered grid system is used at Navier-Stokes momentum equation to calculate flow field effectively using Rhie-Show interpolation method[6]. In non-staggered grid systems, the velocity components on control volume faces are obtained from those on control volume centers using weighted linear interpolation in the physical space as shown in Fig. 4 and eq. (3).

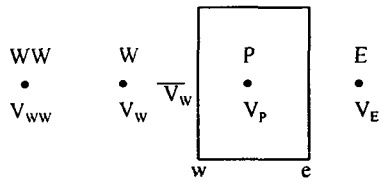

Fig. 4 Control Volume Notation

$$\overline{V}_w = (1 - W_w)V_w + W_w V_p \tag{3}$$

The governing equations used in this study are written in coordinate free tensor notation as follow.

$$\nabla \cdot (\rho V) = 0 \tag{4}$$

$$\frac{\partial \rho V}{\partial t} + \nabla \cdot (\rho V \otimes V) - \nabla \cdot (\mu_{eff} \nabla V) = -\nabla P + \nabla \cdot \left[\mu_{eff} (\nabla V)^T\right] + B \tag{5}$$

$$\frac{\partial \rho k}{\partial t} + \nabla \cdot (\rho V k) - \nabla \cdot \left[(\mu + \frac{\mu_T}{\sigma_k})\nabla k\right] = P' + G - \rho\varepsilon \tag{6}$$

$$\frac{\partial \rho \varepsilon}{\partial t} + \nabla \cdot (\rho V \varepsilon) - \nabla \cdot \left[(\mu + \frac{\mu_T}{\sigma_\varepsilon})\nabla \varepsilon\right] = C_1 \frac{\varepsilon}{k}\left[P + C_3 \max(G,0)\right] - C_2 \rho \frac{\varepsilon^2}{k} \tag{7}$$

$$\mu_{eff} = \mu + \mu_T, \quad \mu_T = C_\mu \rho \frac{k^2}{\varepsilon} \tag{8}$$

$$P' = \mu_{eff}\nabla V \cdot \left[\nabla V + (\nabla V)^T\right] \quad (9)$$

$$G = G_{buoy} = -\frac{\mu_{eff}}{\rho\sigma_p} g \cdot \nabla\rho \quad (10)$$

$$\frac{\partial \rho H}{\partial t} + \nabla \cdot (\rho V H) - \nabla \cdot (K \nabla T) = 0 \quad (11)$$

$$C_1=1.44,\ C_2=1.92,\ C_3=0.0,\ C_\mu=0.09 \quad (12)$$

The fully implicit backward difference time stepping procedure is used for the transient calculation.

$$\frac{\partial \phi}{\partial t} = F(\phi), \quad \frac{\phi^n - \phi^{n-1}}{\Delta t} = F(\phi^n) \quad (13)$$

3.3 Initial and Boundary Conditions

Since Navier-Stokes equation is the mixing of parabolic and elliptic type, initial and boundary conditions for all variables should be specified. The data of reactor coolant mass flow rate, fluid temperature in cold leg and ECC mass flow rate are quoted from the result of safety analysis in the CESSAR-DC (Combustion Engineering Standard Safety Analysis Report-Design Certification) as shown in Figure 5 and 6.

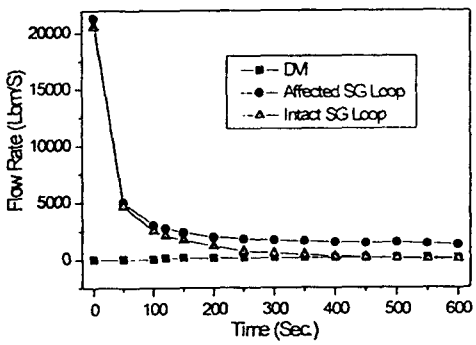

Fig. 5 Flow Rate cited from Safety Analysis Result

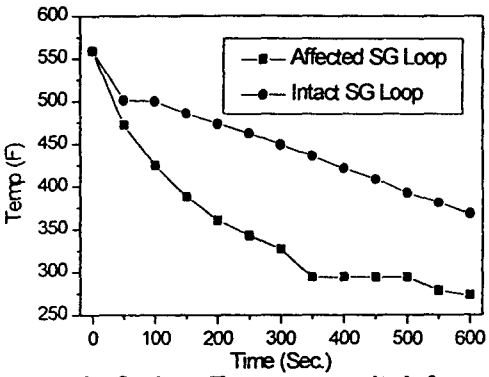

Fig. 6 Coolant Temperature cited from Safety Analysis Result

The temperature of ECC coolant is assumed to be 55F conservatively. The mass flow of ECC coolant depends on the characteristic curve of ECC pump. Initial conditions. 1.19kpsi, 324F, are adopted from the result of safety analysis for MSLB, 570 second after accident initiation.

For the cold leg and DVI nozzle inlet boundary conditions, Dirichlet condition is applied so that all the transport quantities are specified. The RVDC outlet boundary condition is the Neumann condition. Zero gradient of all of the transport quantity in the axial direction is set at the outlet boundary ($\frac{\partial \phi}{\partial z} = z \cdot \nabla\phi = 0$). Adiabatic and no-slip conditions are used at the wall and symmetry condition is applied to the 180° cut wall. User FORTRAN USRBCS with inlet temperature, velocity, k and ε is used to assign transient boundary condition. The inlet values of k and ε is treated as shown in equation (14).

$$k_{inl} = 0.002 V_{inl}^2,\ \varepsilon_{inl} = \frac{k_{inl}^{1.5}}{0.3D} \text{ [6]} \quad (14)$$

In turbulent flow, wall function, eq.

(15)~(18), is used at the near wall regions instead of using extremely fine grids for velocity profile calculation.

$$u^+ = \begin{cases} y^+, for \quad y^+ < y_o^+ \\ \frac{1}{\kappa}\log(Ey^+), fory^+ > y_o^+ \end{cases} \qquad (15)$$

$$y^+ = \frac{(\rho\tau_k)^{1/2}}{\mu}(d-y) \qquad (16)$$

$$\tau_k = \rho C_\mu^{1/2} k \qquad (17)$$

$$y_o^+ = \frac{1}{\kappa}\log(Ey_o^+) \qquad (18)$$

3.4 Calculation Method

In this transient computation, fixed time step and adaptive time step are alternatively used. The time step is automatically controlled by CFX depending on the limited enthalpy residual in the adaptive time step control. The CFX which uses backward and implicit method recommends time step of 1×10^{-2} seconds. However, very small time step (1×10^{-3}~1×10^{-5}) is used in this calculation to obtain well converged results since flow field is complex and temperature difference between coolants is very large. The time step for case 1, 2, 3 and 5 is 1×10^{-3}~1×10^{-4} second and that for case 4 is 1×10^{-4}~1×10^{-5} second.

In general, velocity, mass, k and ε except enthalpy are converged for all the cases when the time step is carefully selected. To get better convergence for enthalpy, under relaxation factor for enthalpy is decreased to 0.4~0.6 for all the cases. The calculation stops when the normalized enthalpy residual becomes smaller than 1×10^{-5}~1×10^{-6} for case 1, 2, 3, 5 and 1×10^{-4}~1×10^{-5} for case 4. Approximately 20~30 iterations were required to obtain converged solution at each time step.

4. Discussions of Results

The outer surface temperature distribution of annulus and velocity vector profile in RVDC of case 1 at 600 seconds after MSLB are shown in Fig. 7 and Fig. 8, respectively. The velocity profile is selected at the center node in RVDC. Figure 9 shows the circumferential temperature distribution at the outer surface of the annulus at the vessel beltline region.

Since most of the ECC flow from the DVI nozzle A flows down to the left side of RVDC outlet, the low temperature distribution at the vessel beltline appears at the location between 10° and 30° from the left symmetry plane (Fig. 7, 9).

The ECC flow from the DVI nozzle B severely affected by the RCS circulation flow from the cold leg B. Most part of the flow from DVI nozzle B moves to upward and turns down to the cold leg A and remaining small portion migrates to the right symmetry plane.

The flow from the cold leg B seems to behave as a flow barrier and most of flow moves down to the right side of RVDC outlet. The mass flow rate through cold leg B is eight times larger than that of DVI as shown in Fig. 5. As a result of this flow pattern, the temperature between the 60°~120° region in the bottom part of the vessel beltline is much higher than that of other regions(Fig. 7, 9).

For certain region the initial condition remains continuously until the end of calculation since the flow from DVI nozzles and cold leg B does not flow into this region. The non-uniform distribution of velocity and temperature in Fig. 7 and 8, may cause large local temperature difference and result in

high thermal stress. However, PTS concern is not a problem in this case, since the lowest temperature is well above RT_{PTS}(98F). The vessel beltline temperature at around 180° region is relatively stable. It can be explained that ECC flow from the DVI nozzle B flows to circumferential direction and mixes very well before reaching vessel belt line.

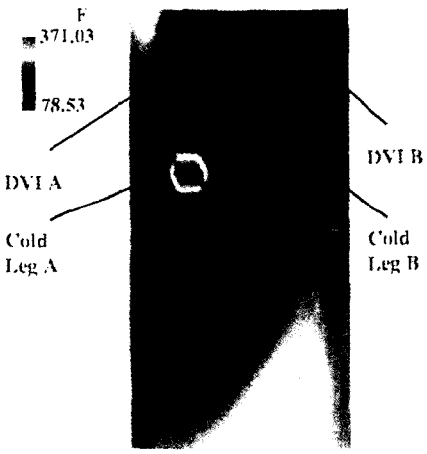

Fig. 7 Annulus Outer Surface Temp. (Case 1)

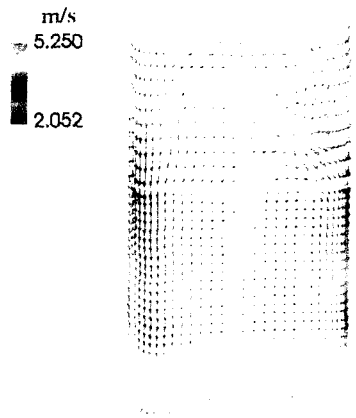

Fig. 8 Velocity Vector in RVDC (Case 1)

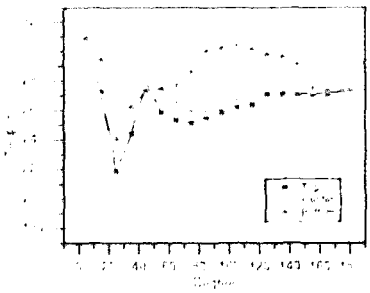

Fig. 9 Vessel Beltline Temp. (Case 1)

The temperature distribution and velocity vector profile for case 2 are shown in Fig. 10~12. The flow patterns are slightly different with those of case 1 because DVI nozzle location is moved as shown in Fig. 2. The coolant through DVI nozzle A flows directly downward direction to the 20°~60° region from left symmetry plane. The water from DVI nozzle B is also severely affected by the RCS circulation flow. Most part of coolant from DVI nozzle B moves to the left side and soon downward direction into the cold leg A and other small part flows directly downward direction into the 130°~180° region.

During this flow process, thermal mixing between the water through DVI and cold leg happens well. Thus, the temperature distribution at the 20°~60° region is less sharpen than that of case 1 and the temperature distribution of vessel beltline center region at 70°~140° is higher than that of case 1.

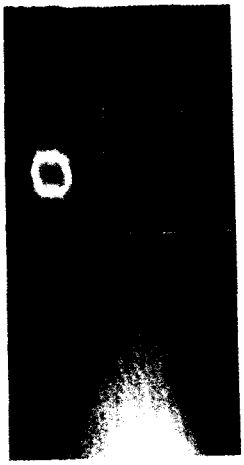

Fig. 10 Annulus Outer Surface Temp. (Case 2)

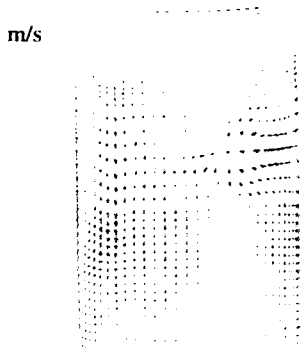

Fig. 11 Velocity Vector in RVDC (Case 2)

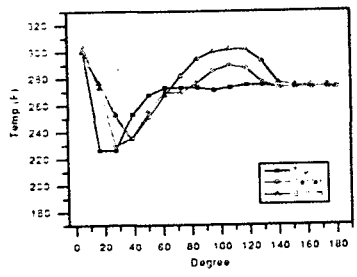

Fig. 12 Vessel Beltline Temp. (Case 2)

The velocity vector profile and temperature distribution for case 3 are shown in Fig. 13~15. The flow patterns are similar to those of case 2. However, Fig. 13 and Fig. 14 show that temperature variation at the vessel beltline is not high as for the case 2. The reason is that thermal mixing between coolants occurs better than for the case 2 due to the short distance between DVI nozzle and cold leg. The coolant from both DVI nozzles flows mainly downward direction about the 20°~60° and 90°~120° so that the temperature around 130° region in the bottom part of the vessel beltline is high.

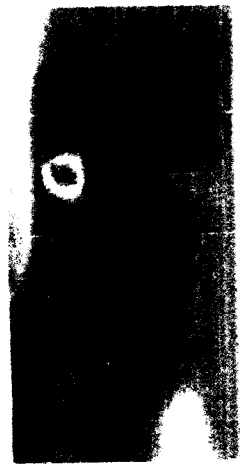

Fig. 13 Annulus Outer Surface Temp. (Case 3)

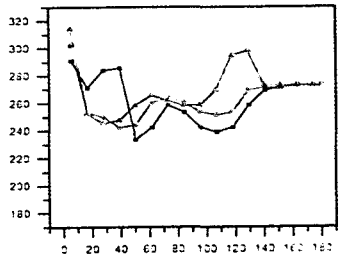

Fig. 14 Vessel Beltline Temp. (Case 3)

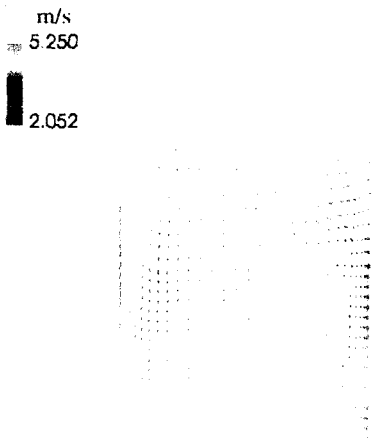

Fig. 15 Velocity Vector in RVDC(Case 3)

The temperature distribution and velocity vector profile for case 4 are shown in Fig. 16~18. The flow patterns are also similar to those of case 2 and 3. The temperature distribution of vessel beltline is more uniform than other cases. By comparing the temperature distribution between the top and bottom of vessel beltline, we can find that the flow from the DVI nozzle B moves to the other symmetry plane while mixing with RCS circulation flow. The reason for the good thermal mixing of coolants may due to the short distance between the DVI nozzle and cold leg.

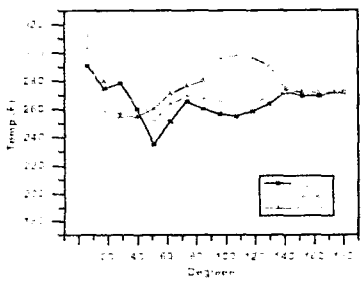

Fig. 16 Vessel Beltline Temp. (Case 4)

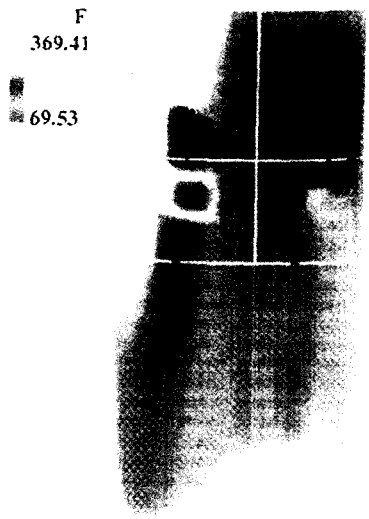

Fig. 17 Annulus Outer Surface Temp. (Case 4)

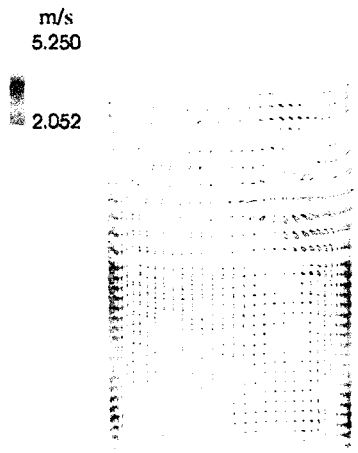

Fig. 18 Velocity Vector in RVDC(Case 4)

Case 5(Fig.19~21) shows that flow pattern and temperature distribution are significantly different from those of case 1, 2, 3 and 4. The coolant from the DVI nozzle A flows to the left side of RVDC outlet with almost no interaction with the cold leg flow, so that the lowest temperature at the vessel beltline appears at around 0° ~ 10° region and the second lowest temperature appears at around 170° ~180° region(Fig. 21). The coolant from DVI nozzle B also moves to the right side of RVDC outlet with a little interaction with the coolant through cold leg B. The lowest temperature is much lower than that of other cases because of the poor fluid mixing. However, the PTS concern is not a problem in this case, too.

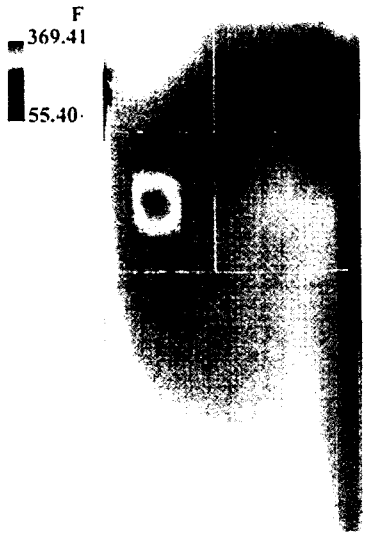

Fig. 19 Annulus Outer Surface Temp. (Case 5)

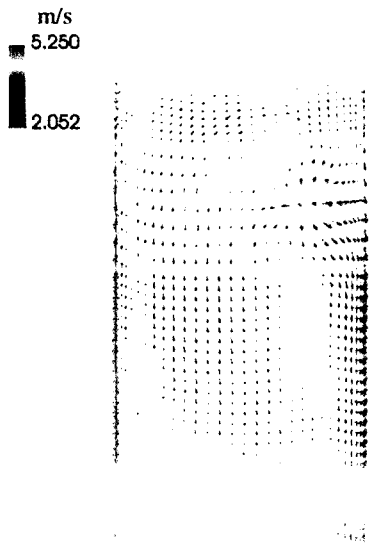

Fig. 20 Velocity Profile in RVDC(Case 5)

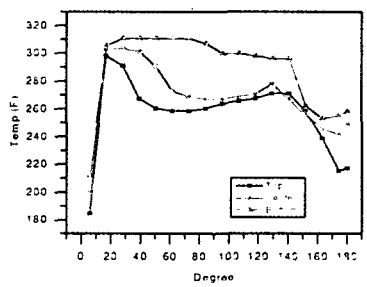

Fig. 21 Vessel Beltline Temp. (Case 5)

5. Conclusions

A numerical study has been performed for the thermal mixing of ECC coolant through DVI with coolant in RVDC to investigate the impact of DVI nozzle location on the PTS and the optimum DVI nozzle location. Five DVI nozzle locations were selected to investigate the effect of DVI nozzle location on thermal mixing in RVDC. The

calculation are obtained by using commercially available computational fluid dynamic code CFX, which solves unsteady three dimensional continuity, momentum, energy equations with various turbulent models under SIMPLE solution algorithm.

The analytical results are as follows. 1) Since the vessel beltline temperature of all cases is much above RT_{PTS}(98F), all case satisfy PTS concern. 2) With regard to temperature distribution, case 3 and 4 show more even distribution. Case 1, 2 and 5 show very low local temperature, and poor thermal mixing. The most uniform temperature distribution of vessel beltline is case 4.

Therefore, it is recommended that the DVI nozzle location should be right above the cold leg nozzle as best as it can. However, final recommendation for optimum DVI nozzle location should be made in consideration of structure integrity, piping arrangement interface as well as thermal mixing..

References

1. ABB-CE Standard Safety Analysis Report for System 80+ Design Certification, ABB Combustion Engineer -ing, 1993
2. C. A. Nielsen, Pressurized Thermal Shock CRT-2 Lecture, ABB Combustion Engineering Interoffice Corresponding, Rep. FSP-88-059, 1988
3. L. P. Litke, B. T, Lubin and F. L. Carpentino, "3-D CFD Model of Reactor Vessel Annulus with DVI", KAIF/KNS Conference, 1992
4. J. H. Cha and H.G. Jun, "An Investigation of Fluid Mixing with Direct Vessel Injection ", Journal of the Korean Nuclear Society Vol. 26, Number 1, March 1994
5. Y. S. Kim, "DVI Design Development for R&D for KNGR" KAERI internal Technical Report, Dec. 1994
6. CFX 4.2 User Guide, UKAEA, 1998
7. Fluent User's Guide Version 4.3, Fluent.Inc, 1996
8. Shoichiro Nakamura, Computational Methods in Engineering and Science, JOHN WILEY & SONS, 1985
9. Suhas V. Patanka, Numerical Heat Transfer and Fluid Flow, McGraw-Hill, New York, 1980
10. Dale A. Anderson, John C. Tannehill and Richard H. Pletcher, Computational Fluid Mechanics and Heat Transfer, McGraw-Hill, New York, 1984
11. Keun-Sun Chang and Byeong-Ho Park, "A Numerical Study on Mixing characteristics of Chemical Injection Tank", Journal of the Korean Nuclear Society Vol. 29, Number 1, pp. 58 ~ 67, February 1997